

Article

# Evidence of Hysteresis Free Ferromagnetic Nature and Significant Magnetocaloric Parameters in FeNi Binary Alloy

Mohit K. Sharma<sup>1</sup>, Akshay Kumar<sup>1</sup>, Kavita Kumari<sup>2</sup>, Su-Jeong Park<sup>3</sup>, Naveen Yadav<sup>3</sup>, Seok-Hwan Huh<sup>4,\*</sup> and Bon-Heun Koo<sup>5,\*</sup>

<sup>1</sup> Mechatronics Research Institute, Changwon National University, Changwon 51140, Republic of Korea

<sup>2</sup> Industrial Technology Research Institute, Changwon National University, Changwon 51140, Republic of Korea

<sup>3</sup> Department of Materials Convergence and System Engineering, Changwon National University, Changwon 51140, Republic of Korea

<sup>4</sup> Department of Mechatronics Conversion Engineering, Changwon National University, Changwon 51140, Republic of Korea

<sup>5</sup> School of Materials Science and Engineering, Changwon National University, Changwon 51140, Republic of Korea

\* Correspondence: hsh1022@changwon.ac.kr (S.-H.H.); bhkoo@changwon.ac.kr (B.-H.K.); Tel.: +82-55-213-2802 (B.-H.K.)

**Abstract:** In this study, our aim is to investigate the structural, magnetic, and magnetocaloric properties of the FeNi binary alloy. The FeNi alloy with Fe<sub>65</sub>Ni<sub>35</sub> composition was prepared by ball milling followed by the annealing and quenching processes. A Rietveld refinement analysis of structural results reveals that this system has coexisting cubic structural phases with a dominant face-centered cubic phase (Fm-3m;γ-FeNi). Magnetization results of this compound indicate the presence of ferromagnetic ordering and the magnetic transition observed around 100 K. Moreover, an Arrott plot study provides information about the order of phase transition, which is found in the second-order near the ordering temperature, whereas first-order nature is also noted in the low-temperature region. The significant magnetocaloric parameters, i.e., magnetic entropy change ( $\Delta S_M \sim 0.495$  J/kg-K) and relative cooling power (88 J/kg), are noted over a wide temperature range. The power law dependency of magnetic entropy change with the applied field is also investigated. Due to their significant magnetocaloric performance over a wide temperature range, these multiphase alloys may be a good candidate for room-temperature to low-temperature magnetic refrigeration.

**Keywords:** Fe-based binary alloy; structural properties; magnetic properties; magnetocaloric properties



**Citation:** Sharma, M.K.; Kumar, A.; Kumari, K.; Park, S.-J.; Yadav, N.; Huh, S.-H.; Koo, B.-H. Evidence of Hysteresis Free Ferromagnetic Nature and Significant Magnetocaloric Parameters in FeNi Binary Alloy. *Magnetochemistry* **2023**, *9*, 8. <https://doi.org/10.3390/magnetochemistry9010008>

Academic Editors: Lotfi Bessais, Bhaskar Das and Renu Choudhary

Received: 13 November 2022

Revised: 9 December 2022

Accepted: 20 December 2022

Published: 26 December 2022



**Copyright:** © 2022 by the authors. Licensee MDPI, Basel, Switzerland. This article is an open access article distributed under the terms and conditions of the Creative Commons Attribution (CC BY) license (<https://creativecommons.org/licenses/by/4.0/>).

## 1. Introduction

In recent times, the search and investigation of magnetic materials have gained paramount importance in the field of magnetism due to their fundamental and practical utility. In order to solve the various energy and thermal management issues in our daily lives, researchers have paid much attention to the magnetic, magnetocaloric, and other promising functional properties of magnetic materials. The magnetocaloric effect (MCE) is the basis of magnetic cooling, which has shown great technological potential due to its environment-friendliness, energy-efficiency, and thermal management nature [1–11]. Various alloys and oxide materials with a significant MCE have been extensively investigated and documented due to their applications in magnetic refrigeration at different temperature regions [6–19]. Materials demonstrating such effects have shown their influence on various physical properties such as entropy, heat capacity, and thermal conductivity, as well as reflecting the transformations taking place in the magnetic material's spin structure [4,5]. The MCE is the intrinsic property of all magnetic materials and is known as magneto-thermodynamic characteristics. On the basis of thermal and magnetic hysteresis, magnetic

materials follow two types of magneto-thermal transitions: first-order transition (FOT) and second-order transition (SOT). The nature of magnetic transition and hysteresis play crucial roles as magnetic cooling is a cyclic process, and hysteresis can reduce the efficiency of the magnetocaloric device. FOT materials have a good MCE in a narrow working temperature span but exhibit temperature and magnetic hysteresis [10–19]; however, SOT materials show a moderate MCE value over a broad working temperature span [10,14,15,19]. This working temperature span affects the essential parameter of the MCE, known as relative cooling power (RCP), i.e., the amount of heat transferred between the hot and cold ends of the thermodynamic cycle [10]. Therefore, materials with a SOT are generally preferred over a FOT due to their low hysteresis nature [1,10–19]. In this regard, researchers focus on investigating the most cost-effective materials that have a MCE with both a FOT and SOT. Rare earth-free transition metal-based materials are documented in such cost-effective categories of caloric materials; in addition, these materials display good magnetic and other related functional properties along with the magnetocaloric effect [6,7,11,20–35]. Different compositions of Fe-M (M = transition metal) alloys have been reported through experimental and theoretical investigations that bring forth fundamental aspects and functions of the MCE phenomenon [11,20–33]. These binary alloys offer significant advantages and potential technological opportunities as various stoichiometries of these alloys can demonstrate remarkable diversity of physical properties.

The series of compounds in the binary alloys  $\text{Fe}_{100-x}\text{M}_x$  are well-known for their magnetic and other related functional properties such as magnetocaloric and magnetoresistance [6,22,31–33]. The crystal structure and composition of dopant play an important role in determining the physical properties of these binary alloys. The phase diagram studies have revealed that binary alloys exhibit various coexisting crystallographic phases [36–39]. These phases mainly depend on the stoichiometric ratio of the constituent elements and the synthesis process, such as alloying, nanocrystallization, annealing, quenching, and heat treatment [28,30–33]. These parameters can also be used in FeNi systems to see their effects on physical properties such as the MCE and the order of phase transitions. FeNi systems demonstrate low- and high-temperature magnetic properties, which depend on the nature of the structural phase of the system [6,24,26,27,33,40,41]. It was reported that FeNi systems with coexisting multiphase, i.e., face-centered cubic, body-centered cubic, and spinel, have better MCE parameters over a broad temperature span [28]. In addition, not only do coexisting crystalline phases occur in these systems, but the coexistence of magnetic phases, i.e., antiferromagnetic and ferromagnetic, was also reported in the literature [41–44]. Thus, the existing literature advocates that the phase fractions or lattice disorders collectively control the magnetocaloric parameter, the broadness of the magnetic transition, and the disordered derived exchange interactions. Moreover, such an investigation may provide a good understanding of the technological and fundamental aspects.

In this manuscript, we are attempting to investigate magnetic and magnetocaloric properties driven by the coexistence of crystallographic phases in the  $\text{Fe}_{65}\text{Ni}_{35}$  binary systems. The structural results reveal that there is no oxide phase in the studied compound; however, it exhibits a multiphase nature with the dominance of the face-centered cubic (Fm-3m) phase along with body-centered cubic (Im-3m) and minute fractions of tetragonal (P4/mmc) phases. Temperature and applied field-dependent magnetization results reveal the evidence of a hysteresis-free ferromagnetic state at low temperatures (~100 K) in the studied compound. The SOT nature of the material around the magnetic ordering temperature is evident in an Arrott plot study; however, the compound also has a FOT in the low-temperature region. Magnetocaloric properties in terms of isothermal magnetic entropy change ( $\Delta S_M$ ) and relative cooling power (RCP) are also investigated. The results demonstrate that this compound has a significant  $\Delta S_M$  over a wide temperature span and displays good RCP values. The obtained values of MCE parameters are comparable to those of promising refrigerant materials in this temperature range. We are also trying to investigate the magnetic nature of the compound by observing the field-dependent magnetic entropy change followed by a power law behavior ( $\Delta S_M \sim H^n$ ). The value of exponent (n)

indicates the existence of mixed magnetic correlation, i.e., the antiferromagnetic correlation found within the ferromagnetic states. Such coexistence may arise due to the multiphase nature of the studied compound. Therefore, the significant values of MCE parameters and the absence of hysteresis in the whole measured temperature range satisfy the important criterion for a magnetic refrigerant material.

## 2. Materials and Method

FeNi binary alloys with the composition Fe<sub>65</sub>Ni<sub>35</sub> were synthesized by ball milling and quenching. For this, we have taken Fe and Ni powders, procured from Sigma Aldrich (Sigma Aldrich, St. Louis, MO, USA; purity  $\geq$  99.6%), as starting reagents. First, we mixed both powders and put the mixture in a planetary ball mill for alloying in an ethanol medium (dimension of ball mill container 250 mL, milling speed 600 rpm, ball diameter 5 mm, and powder-to-ball ratio 1:3). The milling process was carried out in the following steps: the milling on time was 15 min and off time was 5 min. The same steps were used periodically up to a 24 h milling time. After milling, the sample was taken out of the ball mill container and put in the oven at 100 °C until we obtained the fine dry powder. Further, the powder sample was molded into a cylindrical pellet with diameter 10 mm and thickness 2 mm with the hydraulic press by applying 15 Mpa for 15 min. The pellet was kept in the vertical furnace supplied with a controlled flow of hydrogen (99.999%) gas at 950 °C for 6 h, followed by the quenching in silicon oil (as the hydrogen supply was completely cut off). We used the pellet piece for further investigations. The structural characterization and phase analysis of the alloy were carried out through X-ray diffraction (XRD) and recorded with a PANalytical (Malvern, UK) X-pert Pro-diffractometer containing a Cu-K $\alpha$  X-ray radiation ( $\lambda = 1.54 \text{ \AA}$ ) source. The microstructure of the studied compound was investigated by a scanning electron microscope (SEM; JSM-6510, Jeol, Tokyo, Japan), and the elemental composition was checked with an energy dispersive X-ray spectroscope (EDAX) installed in the SEM instrument. The quenched sample's magnetic properties were obtained from the vibrating sample magnetometer option of the cryogen-free Versa Lab physical properties measurement system (PPMS) by Quantum Design (Quantum Design, San Diego, CA, USA). Magnetocaloric parameters in terms of isothermal magnetic entropy change and relative cooling power (RCP) are derived from the isothermal magnetization data, calculations, and protocol adopted from the literature [18,33,45].

## 3. Results and Discussion

### 3.1. Structural Study

Figure 1a shows the X-ray diffraction pattern for the quenched FeNi binary alloy. From the initial analysis and comparison with the literature, the positions of all diffraction peaks matched with the face-centered cubic (space group = Fm-3m) and body-centered cubic (space group = Im-3m) phases of the FeNi alloy [27,33,41]. Furthermore, the XRD pattern of this sample exhibits a few diffraction peaks that are not aligned with the peak positions of both the cubic phases, suggesting the presence of additional crystallographic phases. In order to identify the accurate crystallographic nature of the studied compound, a Rietveld refinement analysis was performed using FullProf Suite software [46,47]. For this, initially we performed refinement with two phases (Fm-3m and Im-3m) by involving a pseudo-Voigt peak shape function, but the resulting calculated patterns (not shown here) did not provide good agreement with the observed XRD pattern. Rodríguez et al. observed Fm-3m and P4/mmm crystallographic phases through in-depth XRD and X-ray absorption experiments in the ball-milled FeNi system [48]. Therefore, we performed the refinement by considering various combinations of the different crystallographic phases (structure and space group) and peak shape functions. Finally, the goodness-of-fit and values of R-factors between the observed and calculated patterns were significantly improved with the Pearson VII peak shape function and three phases, i.e., Fm-3m (face-centered cubic), Im-3m (body-centered cubic), and phase I4/mmm (tetragonal). The resulting refinement diffraction pattern is shown in Figure 1a. The refined structural parameters and phase percentage

obtained by a Rietveld fitting are summarized in Table 1. From the phase diagram study, generally, FeNi-based systems have contained different phases depending on the Fe/Ni composition, heat treatments, as well as nucleation and growth mechanisms [49–54]. In the present study, the weight fraction of the third (P4/mmm) phase is very low, i.e., 1.55 % (as shown in Table 1); this phase is also reported in the ball milled FeNi system [48]. These additional phases may form during the annealing/quenching process when the sample cools from its high temperature to room temperature. Additionally, multiple phases in the FeNi system are not uncommon; literature reports advocate that these systems often establish more than one crystallographic phase [27,33,48,50–52], and some groups even reported the occurrence of three phases simultaneously [28]. Moreover, on behalf of the theoretical, experimental, and phase diagram studies, it is a well-known fact that these binary alloys are found in different types of structural unit cells, including face-centered, body-centered, tetragonal, and hexagonal [25,26,31,46–48], which are completely consistent with the present study. In order to analyze the microstructure, the sample is characterized with SEM, and the resulting micrograph of the quenched sample is shown in Figure 1b. The microstructure clearly displays two contrasting regions forming a light gray matrix with dark patches in between. This advocates for the occurrence of two separate phases in the compound; intrigued by this finding, we carefully checked the elemental composition of both regions through EDAX, as shown in Table 2. The EDAX results indicate equal amounts of Fe and Ni from both areas, which signify that both regions belong to FeNi phases. It is well established in the available literature that cubic phases of FeNi consist of equimolar amounts of Fe and Ni elements [33,40,43,48], which is consistent with the present observations. Conversely, the occurrence of contrasting regions in the micrographs could be simply attributed to the difference in the densities and packing fractions of the cubic phases of FeNi. Nevertheless, the microstructural analysis confirmed that the two contrasting regions contain micrograins of at least two unresolved cubic phases. However, we did not find significant signatures of the third phase in the microstructure, which could be due to the minute amount of this phase in the sample.

### 3.2. Magnetization Study

Figure 2a shows the temperature-dependent magnetic response curve obtained under zero-field-cooled cooling (ZFC), field-cooled cooling (FCC), and field-cooled warming (FCW) conditions at the 100 Oe applied field. From the obtained magnetization curves, it has been observed that, on decreasing the temperature, a small bifurcation between the ZFC and FCW plots is noted around 200 K, increasing up to the lowest measured temperature. The exact magnetic ordering temperature, i.e., around ~100 K, is shown in the derivative of ZFC magnetization (shown in Inset 1 of Figure 2a). Moreover, the ZFC and FC curves are not merged completely even at the highest possible measured temperature, which clearly indicates that this compound does not completely achieve the paramagnetic state. Even though most reports on FeNi compounds state that they exhibit magnetic ordering above room temperature or at very high temperatures [6,24–28,32,33], a few compositions, such as the NiFe<sub>2</sub> metallic compound, show the ordering around 138 K [40]. In our case, it arises at a comparatively lower temperature, and, interestingly, this magnetic ordering is shifted towards higher temperatures with increasing applied field (Insets I and II of Figure 2a), suggesting the dominance of ferromagnetic nature in this compound. The low-temperature magnetic ordering can originate due to the dominance of the Fm-3m phase; other phases do not affect the magnetic behavior as much because they have high-temperature magnetic ordering. However, competition between both phases may adjust the effective exchange interactions and provide a broadening to the magnetic transition that is enhanced with the applied field, as evident in the insets of Figure 2a. This type of behavior is not unusual in Fe-based binary systems. Several microscopic magnetic studies exist in the literature where these systems have additional magnetic states along with ferromagnetic, low-temperature antiferromagnetic, ferrimagnetic, and glassy magnetic states [38–41,49]. Additionally, the FCC and FCW curves demonstrate a slight deviation between them, which

confirms the presence of weak thermal hysteresis in the sample. Furthermore, an interesting feature—a crossover in ZFC and FCC curves—has also been observed, indicating the presence of various magnetic states in the sample.

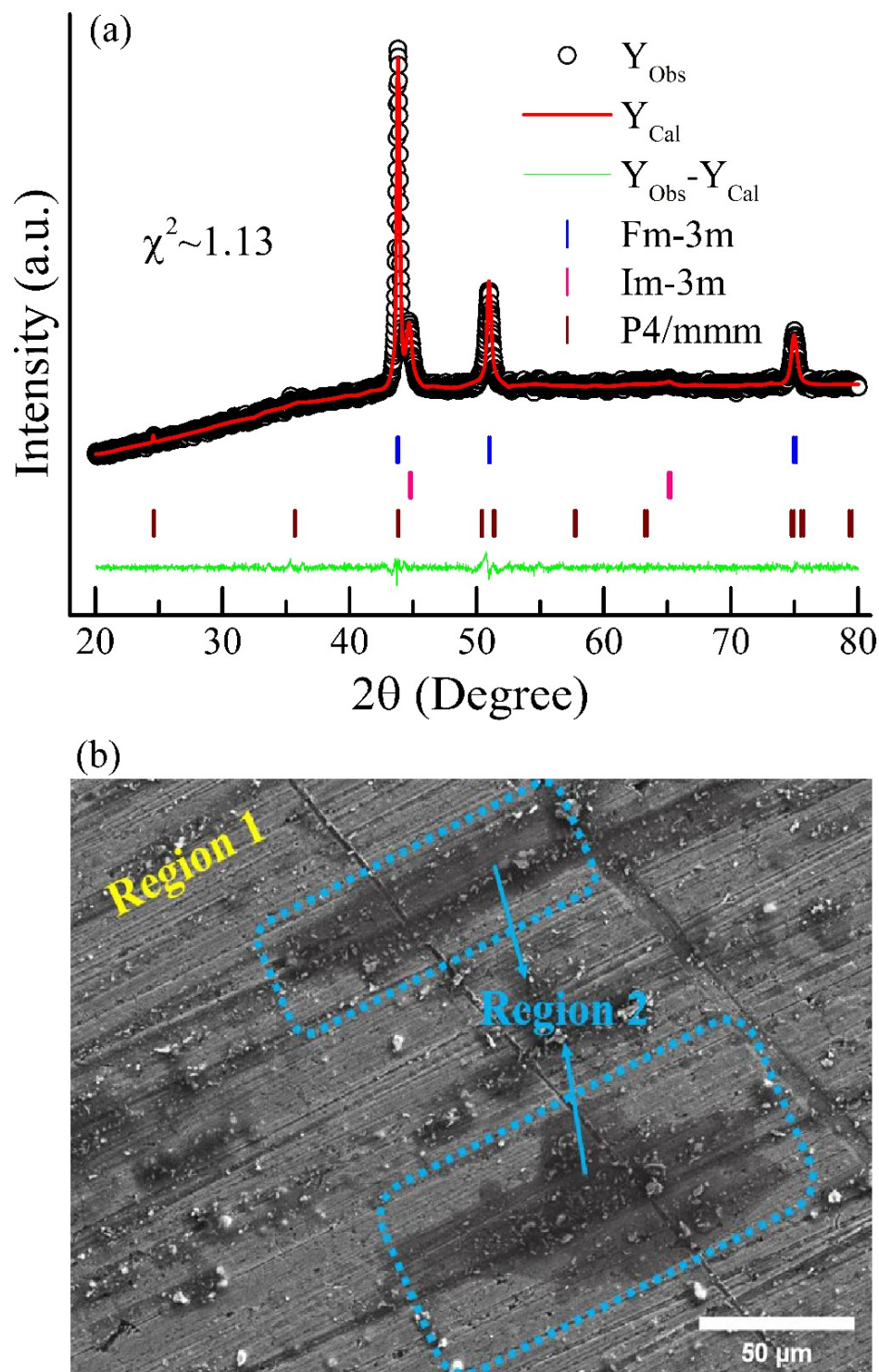


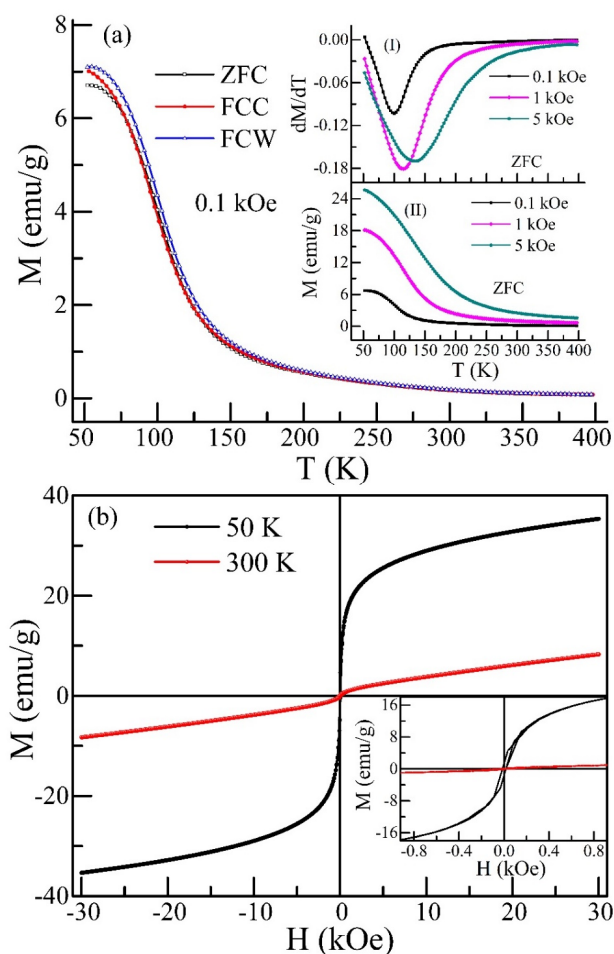
**Figure 1.** Structural and microstructure of studied compounds: (a) Rietveld analysis of X-ray diffraction pattern for the  $\text{Fe}_{65}\text{Ni}_{35}$  alloy. Bragg position of phase 1 (blue color) for the Fm-3m phase; Bragg position of phase 2 (Pink color) for the Im-3m phase; Bragg position of phase 3 (Wine color) for the P4/mmm phase. (b) SEM micrograph for the studied alloys.

**Table 1.** Structural and fitting parameters obtained from a Rietveld refinement.

Refined Parameters	Cubic Fm-3m (Fe <sub>65</sub> Ni <sub>35</sub> )	Cubic Im-3m (Fe <sub>70</sub> Ni <sub>30</sub> )	Tetragonal I4/mmm (FeNi)
<i>a</i> (Å)			2.5161(3)
<i>b</i> (Å)	3.5818(4)	2.8630(5)	2.5161(3)
<i>c</i> (Å)			3.6212(4)
Phase fraction (%)	61.96(0.93)	36.49(0.59)	1.55(0.25)
Goodness-of-fit		1.13	
Bragg R-factor	2.31	2.1	10.51
RF-factor	1.10	1.2	12.13

**Table 2.** Elemental composition of both regions obtained from the EDAX analysis.

Element	Line Type	K Ratio	Wt%	Wt% Sigma
<b>Region 1</b>				
Fe	K series	0.02858	69.15	0.57
Ni	K series	0.01178	30.85	0.57
<b>Region 2</b>				
Fe	K series	0.02700	74.73	0.51
Ni	K series	0.00844	25.27	0.51

**Figure 2.** (a) Temperature-dependent magnetization plot in various conditions, i.e., zero-field-cooled cooling (ZFC), field-cooled cooling (FCC) and field-cooled warming (FCW) of Fe<sub>65</sub>Ni<sub>35</sub> alloy. **Inset I:** M-T plot at different fields. **Inset II:** Derivative of M-T plot at different fields. (b) Magnetic hysteresis loop at 50 K and 300 K for Fe<sub>65</sub>Ni<sub>35</sub>. **Inset:** M-H plot enlarged view to see the magnetic hysteresis.

In order to obtain better insight into the magnetic nature of the compound, investigating the isothermal magnetization as a function of the applied magnetic field is necessary, along with conducting a temperature-dependent magnetization study. Isothermal magnetization ( $M$ ) behavior as a function of the applied magnetic field ( $H$ ) was obtained up to  $\pm 30$  kOe in the temperature range of 50 K to 400 K. Representative curves at different temperatures (50 K and 300 K) for  $\text{Fe}_{65}\text{Ni}_{35}$  are shown in Figure 2b. The shape and nature of the magnetic isotherms display that this compound exhibits a hysteresis-free magnetic state, either because it is soft ferromagnetic or a mixture of antiferromagnetic/ferrimagnetic along with ferromagnetic. Such a nature is expected in multiphase systems because of their different crystallographic sizes and/or presence of various magnetic exchange interactions. The room temperature plot also shows a small amount of ferromagnetic character, and this effect is analogous to our temperature-dependent results, where this compound does not attain a complete paramagnetic state.

In the following section the magnetic state of the compound is discussed with the scientific reasoning based on the available literature. FeNi alloys mostly have magnetic ordering at high temperatures, which is known to be ferromagnetic in nature [6,27,28,33,54]. However, several theoretical and experimental investigations also determined the antiferromagnetic or ferrimagnetic and glassy nature of the magnetic state in Fe-based binary alloys [41–44,53,54]. Therefore, such a magnetic state might stabilize in the face-centered cubic matrix at the low-temperature region, where small-scale FeNi clusters could be developed and compete with other phases. The existence of these face-centered cubic iron clusters may be responsible for different magnetic states in the sample. In addition, different magnetic (low spin and high spin) phases also play a significant role in the occurrence of the various magnetic states [41,43,44]. It depends on the crystallographic (face-centered, tetragonal, and body-centered) nature of the compound. The available literature suggests that if the face-centered phase exists in a high spin phase, it becomes ferromagnetic, while the low spin case demonstrates antiferromagnetism below 20 K [41,54]. However, a few groups have reported that antiferromagnetism appears in face-centered cubic iron below 70 K [41,54]. The low value of magnetization also supports the coexistence of a low spin phase in the compound prepared in this study. In the present case, we obtained a multiphase compound (as discussed in the structural study), so there is a possibility for a significant amount of face-centered FeNi low spin phase along with other foreign phases to precipitate during the annealing and quenching process. Competition between these phases may provide the driving force for originating the different magnetic correlations and developing the different magnetic states in the sample, which is clearly evident in the microscopic methods mentioned elsewhere [42].

### 3.3. Arrott Plot Study

In order to confirm the nature of the transition in the vicinity of magnetic ordering, the  $H/M$  vs.  $M^2$  plot is derived from the virgin magnetic isotherms (Figure 3a). Both resulting plots are shown in Figure 4. This plot is known as an Arrott plot (Figure 3b) and exhibits negative and positive slopes for first- and second-order phase transitions. As noted from the figure and Banerjee's criterion of phase transition [55], a positive slope is observed near the magnetic ordering temperature, indicating that this phase transition is second-order. However, the curvature of the plot is changed below the magnetic ordering temperature. This curvature further increases with decreasing temperatures. Below the magnetic ordering temperature, it appears that the sample is trying to achieve a first-order transition. To confirm the exact temperature where the first-order transition started, we analyzed the Arrott plot data in terms of magnetic free energy  $F(M, T)$ . Landau's expression for free energy is written as [15,56]:

$$F(M, T) = \frac{C_1}{2}M^2 + \frac{C_3}{4}M^4 + \frac{C_5}{6}M^6 + \dots - HM \quad (1)$$

where  $C_1$ ,  $C_3$  and  $C_5$  are the Landau coefficients; these coefficients are calculated by using the following equation [15]:

$$H/M = C_1(T) + C_3(T)M^2 + C_5(T)M^4 \quad (2)$$

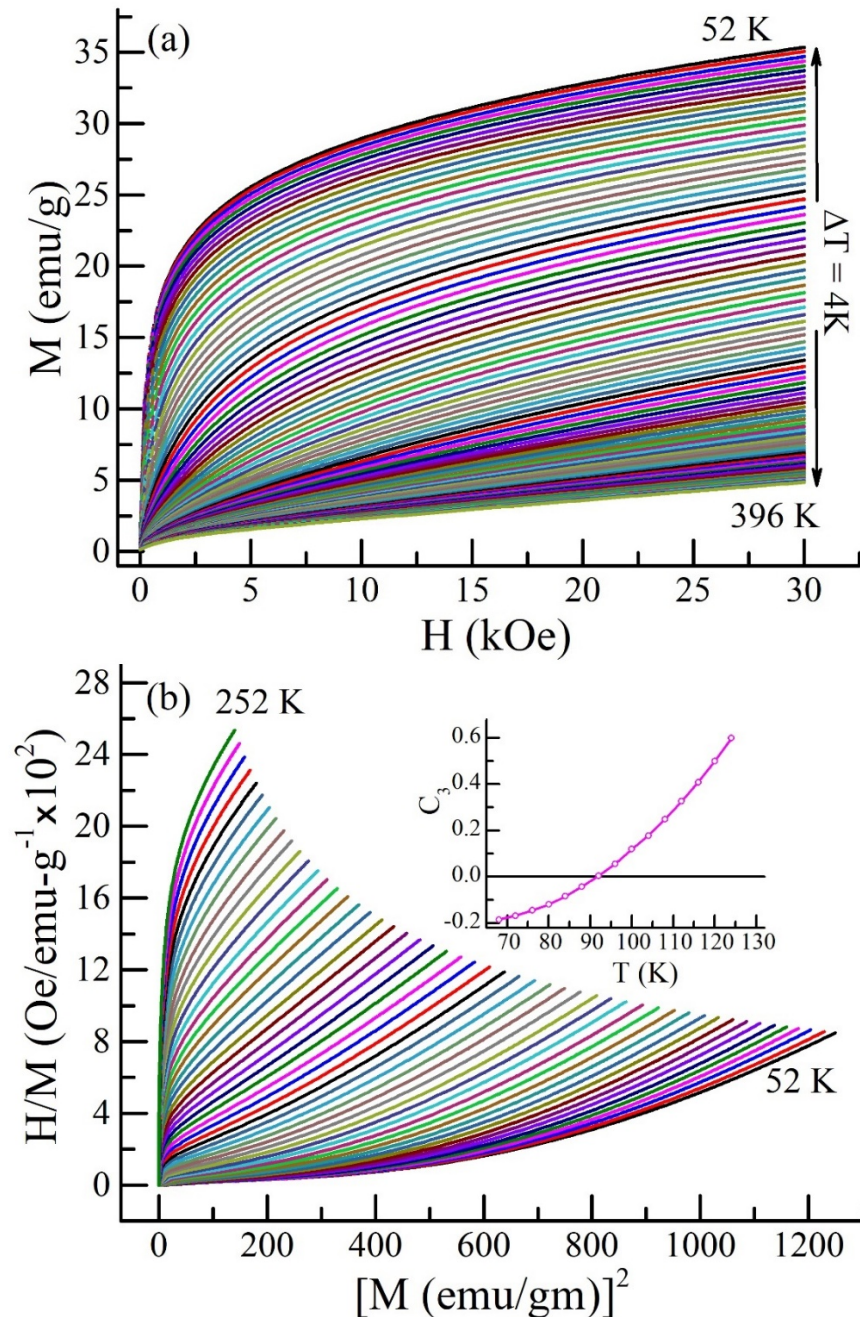


**Figure 3.** (a) Virgin isothermal magnetization curve at different temperatures for  $\text{Fe}_{65}\text{Ni}_{35}$ . (b) Arrott plot, derived from virgin magnetic isotherms, at different temperatures for  $\text{Fe}_{65}\text{Ni}_{35}$ . **Inset:**  $C_3$  vs.  $T$  plot (obtained from the non-linear curve fitting by using Equation (2)) for  $\text{Fe}_{65}\text{Ni}_{35}$ .

The coefficient  $C_3$  determines the order of phase transition; it has a positive or negative value for the second-order and first-order, respectively [15]. We have calculated the value  $C_3$  from the  $H/M$  vs.  $M^2$  plot fitted in Equation (2). The calculated values were plotted as a function of temperature (shown in Inset of Figure 3b). The curve shows a positive value above 88 K; below this, it changes its sign and converts into a negative value. Below 88 K, the studied material follows the first-order nature of phase transition. From the above

analysis, it is apparent that this compound has two types of phase transitions. Such results are not uncommon in binary alloys. FeNi binary systems also have an antiferromagnetic nature at low temperatures [41,42,44,54]. The origin of this first-order transition may arise due to the presence of a small antiferromagnetic correlation within the ferromagnetic correlation. These results make an analogy with our magnetization results.

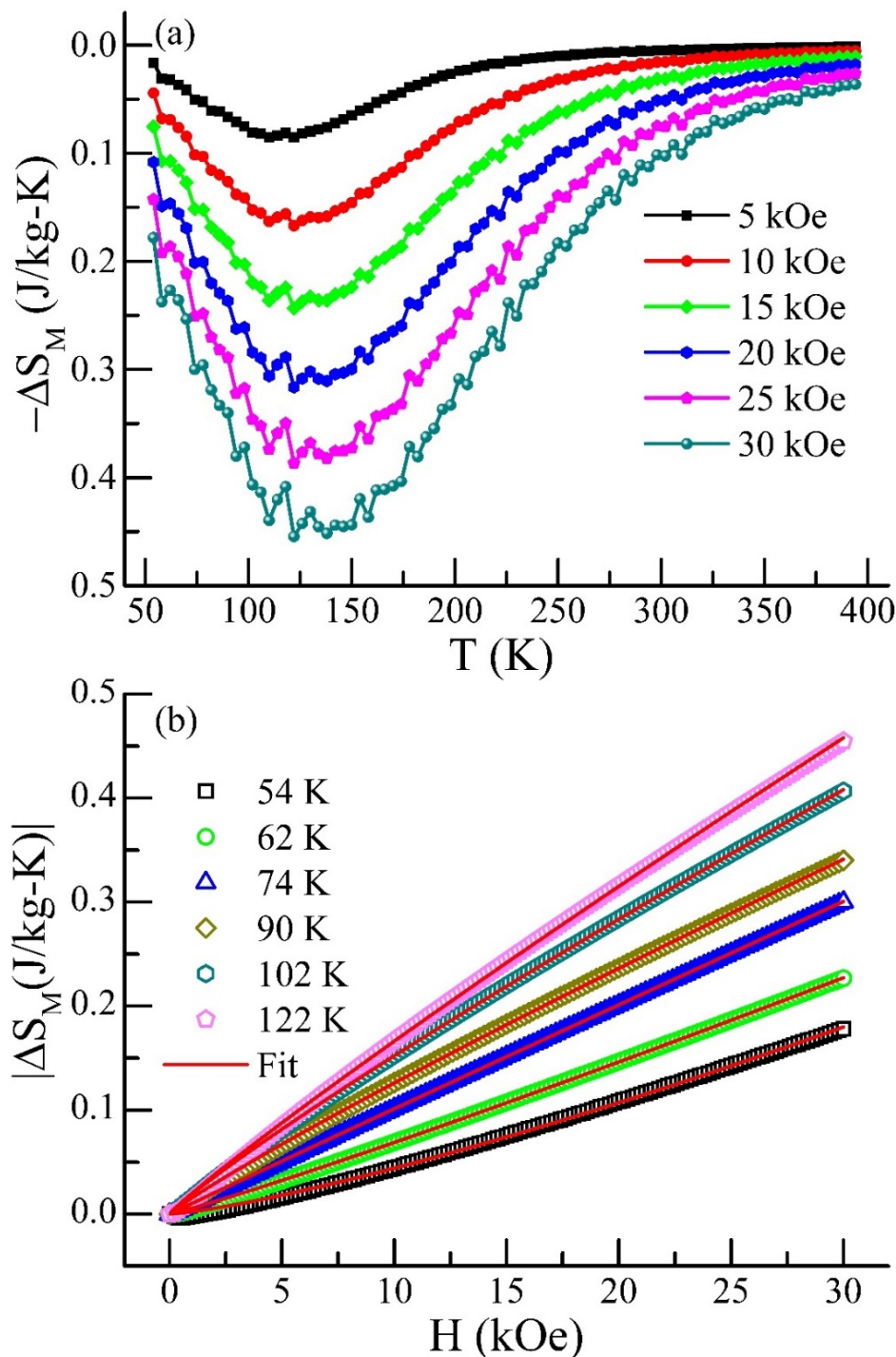


**Figure 4.** Temperature and applied field-dependent isothermal magnetic entropy change ( $\Delta S_M$ ) derived from virgin magnetic isotherms: (a)  $\Delta S_M$  vs.  $T$  plot at different applied field changes for  $\text{Fe}_{65}\text{Ni}_{35}$ . (b)  $\Delta S_M$  vs.  $H$  plot with power law fitting ( $\Delta S_M \sim H^n$ ) at different temperatures for  $\text{Fe}_{65}\text{Ni}_{35}$ . Data and fitting are shown in the symbols and solid lines, respectively.

### 3.4. Magnetocaloric Study

We further investigated the sample by measuring the temperature and field response of the magnetocaloric effect in terms of  $\Delta S_M$  and RCP. The  $\Delta S_M$  is derived from the magnetic isotherms using a similar procedure as described in the literature reports [31,42]. Figure 4a displays the temperature response of  $\Delta S_M$  at different fields. FeNi systems have shown a considerable amount of the  $\Delta S_M$  over a wide temperature range of 54 to 275 K, with a maximum value of  $\sim -0.495$  J/kg-K. Here, we observed that the  $\Delta S_M$  curve demonstrates a slight shift in peak temperature (where  $\Delta S_M$  have maximum value) towards higher temperature compared with magnetic ordering temperature; this is not uncommon in first- and second-order coexisting phase systems; similar nature is also reported in the literature [15,19]. From the viewpoint of the  $\Delta S_M$  value, we get a significant value in such binary systems. To some extent, this compound has a large value of  $\Delta S_M$  from the previously reported FeNi system [33], even though it has a small magnetization value ( $M = 40$  emu/g). However, it shows some large  $\Delta S_M$  values because it exhibits a larger change in magnetization ( $\Delta M/\Delta T$ ), which was crucial in the  $\Delta S_M$  calculations. In addition, mixed phases, either crystallographic or magnetic (first- or second-order), provide the driving force for broadening magnetocaloric parameters in this compound. Moreover, the compound does not exhibit magnetic hysteresis in this temperature range, satisfying another essential criterion for a magnetic refrigerant material. As observed from the resulting curve, the  $\Delta S_M$  vs. temperature curve was shown to be asymmetric around the peak temperature. This behavior occurs in those compounds that show the absence of long-range ordering [1,15,19] and spin fluctuations [1,15,57]. To identify this, we tried to fit the  $\Delta S_M$  vs. applied field curve with spin fluctuation fitting as reported in the literature [1,53]. We did not achieve the best fit because it was found to be good in the paramagnetic region, but in our case, FeNi systems have a paramagnetic phase at very high temperatures; therefore, we discarded the spin-fluctuation nature of this compound.

To understand the intrinsic nature of the sample, we fitted the field response of the  $\Delta S_M$  curve with a power law fitting  $\Delta S_M \sim H^n$  [15,16,31,54,55]. Figure 4b displays the resulting plot for the sample at different temperatures. All of the curves near the magnetic ordering temperature exhibit power law behavior, with exponent  $n$  ranging between 0.89 and 1.7 as determined by power law fitting. The present exponent values are higher than those obtained in ferromagnetic systems, i.e., 0.66 [16,54,55], while they get less value from the antiferromagnetic system,  $\sim 2$  [17,18,33,58,59]. These values of  $n$  clearly suggest that this sample has mixed magnetic states that are ferromagnetic and antiferromagnetic in nature. Interestingly, it was observed from the curve fitting that this power law behavior slightly deviates at a low applied field (up to 5 kOe) below 70 K. Additionally, the value of  $n$  shows an increasing pattern as the temperature decreases. The behavior mentioned above might be due to the dominance of either first-order natural magnetic transitions or antiferromagnetic correlations within the ferromagnetic correlations. The antiferromagnetic nature of the FeNi system at low temperatures is reported theoretically and experimentally in the literature [41,43,44]. Therefore, this compound has a mixed antiferromagnetic and ferromagnetic magnetic state, which can originate due to the mixed crystallographic phases. The antiferromagnetic correlation within the ferromagnetic states and vice versa is well reported in the literature [18,19]. Such weak antiferromagnetism and ferromagnetism originate due to changes in the spin alignment of the sample, governed by the various crystallographic or magnetic clusters present in the sample. An Arrott plot study also supports the existence of first- and second-order natures in the studied compound.

In order to check the practical utility of any material that can be used as a magnetic refrigerant, the relative cooling power (RCP) is an important parameter that needs to be examined. It measures the portion of heat transfer between cold and hot reservoirs in an ideal refrigeration cycle. RCP is calculated as the product of maximum  $\Delta S_M$  ( $\Delta S_M^{\max}$ ) and the full width of the half-maximum of the peak in  $\Delta S_M$  ( $\Delta T_{\text{FWHM}}$ ) [10].

$\Delta S_M$  ( $\Delta S_M^{\max}$ ) and the full width of the half-maximum of the peak in  $\Delta S_M$  ( $\Delta T_{FWHM}$ ) [10,15,33]:

$$RCP = \Delta S_M^{\max} \times \delta T_{FWHM} \quad (3)$$

Here,  $\delta T_{FWHM} = T_{hot} - T_{cold}$ ,  $T_{hot}$  and  $T_{cold}$  are the temperatures corresponding to the half-maximum value of the  $\Delta S_M$  peak value around both sides of the temperature axis. The RCP value as a function of the applied field change is displayed in Figure 5a. At the maximum applied field ( $\Delta H = 30$  kOe), the RCP value is 88 J/kg. The observed values are comparable to other reported magnetic refrigerants. Figure 5 shows that both RCP (Figure 5a) and  $\Delta S_M$  (Figure 5b) values do not show any sign of saturation up to the 30 kOe applied field; enhanced performance can be anticipated at higher applied fields. We also try to fit the  $\Delta S_M$  and RCP peak values, at different applied fields, with power law fitting. The exponent value indicates that this compound shows a coexisting magnetic correlation. Therefore, coexisting phase formation again reaffirms and makes an analogy with magnetic and Arrott plot results.

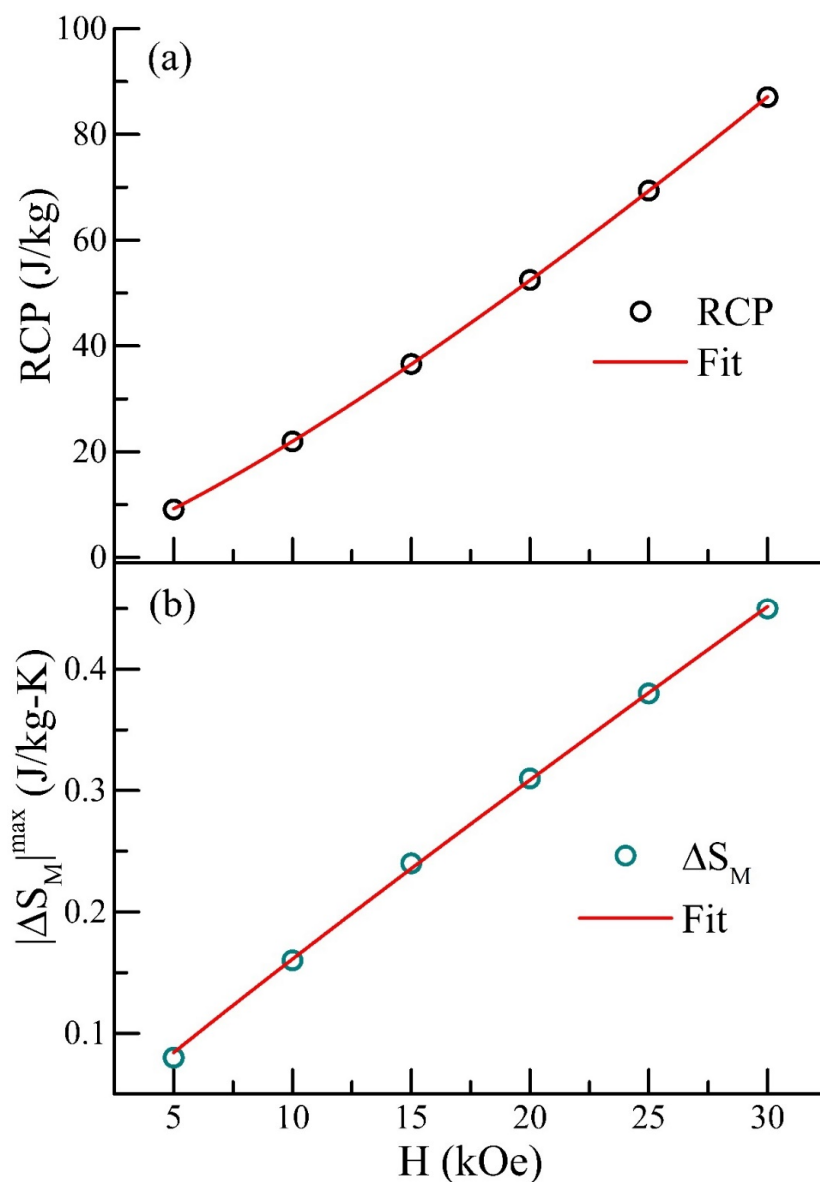


**Figure 5.** Magnetocaloric parameters as functions of applied magnetic field change: (a) RCP vs.  $H$  plot; (b)  $\Delta S_M^{\text{Peak}}$  vs.  $H$  plot. Power law fitting ( $\sim H^n$ ) is displayed by solid line.

#### 4. Conclusions

In summary, we present a systematical investigation of the structural, magnetic, and magnetocaloric studies of the Fe<sub>65</sub>Ni<sub>35</sub> alloy. A Rietveld refinement analysis of structural results reveals the coexistence of Fm-3m, Im-3m, and P4/mmm crystallographic phases. Temperature and magnetic field response of magnetization results confirm the ferromagnetic ordering at the low-temperature region, which is governed by the coexisting nature of the crystallographic phase. The second- and first-order natures of the magnetic ordering are also confirmed by an Arrott plot and Landau expression of free energy. Results demonstrate that the second-order nature of the sample is found near the magnetic ordering temperature; at the same time, the first-order nature was also observed below 88 K. Significant magnetocaloric parameters over a wide temperature span are also observed in temperature-dependent magnetocaloric studies. The short-range magnetic exchange interactions with mixed magnetic correlations are reaffirmed by the power law behavior of field-dependent magnetic entropy change. The applied field-dependent  $\Delta S_M$  and RCP confirm the non-saturated nature of the compound. Therefore, based on the above investigations, the coexisting phase-controlled magnetic and magnetocaloric investigations of these alloys are beneficial to understanding the fundamental and technological aspects of such magnetocaloric materials.

**Author Contributions:** Conceptualization, M.K.S. and B.-H.K.; Methodology, M.K.S.; Software, M.K.S. and A.K.; Validation, S.-H.H. and B.-H.K.; Formal analysis, M.K.S., A.K., K.K. and B.-H.K.; Investigation, M.K.S. and B.-H.K.; Resources, B.-H.K.; Data curation, S.-J.P. and N.Y.; Writing—original draft, M.K.S.; Writing—review & editing, M.K.S., A.K., K.K. and B.-H.K.; Visualization, S.-H.H. and B.-H.K.; Supervision, B.-H.K.; Project administration, B.-H.K.; Funding acquisition, B.-H.K. All authors have read and agreed to the published version of the manuscript.

**Funding:** This research was supported by the Basic Science Research Program through the National Research Foundation of Korea (NRF) and funded by the Ministry of Education (No. 2021R111A3049533). This research was funded by the convergence research financial program for instructors, graduate students, and professors in 2022. MKS acknowledges the Mechatronics Research Institute at Changwon National University, Changwon, Republic of Korea. This research is also funded by the financial program for self-directed research capacity in 2022.

**Institutional Review Board Statement:** Not Applicable.

**Informed Consent Statement:** Not Applicable.

**Data Availability Statement:** Data will be made available on request.

**Acknowledgments:** The authors acknowledge the experimental facilities of the central lab at Changwon National University, Changwon, Republic of Korea. MKS acknowledges the Mechatronics Research Institute at Changwon National University, Changwon, Republic of Korea.

**Conflicts of Interest:** The authors declare that they don't have any known conflict of interest.

#### References

1. Tishin, A.M.; Spichkin, Y.I. *The Magnetocaloric Effect and Its Applications*; CRS Press: Boca Raton, FL, USA; Taylor and Francis Group: Didcot, UK, 2003; ISBN 978-1-4200-3337-3.
2. Pecharsky, V.K.; Gschneidner, K.A. Advanced magnetocaloric materials: What does the future hold? *Int. J. Refrig.* **2006**, *29*, 1239–1249. [[CrossRef](#)]
3. Bruck, E. Developments in magnetocaloric refrigeration. *J. Phys. D Appl. Phys.* **2005**, *38*, R381. [[CrossRef](#)]
4. Kitanovski, A.; Tusek, J.; Tomc, U.; Plaznik, U.; Ozbolt, M.; Poredos, A. *Magnetocaloric Energy Conversion: From Theory to Applications*; Springer International Publishing: Basel, Switzerland, 2015; ISBN 978-3-319-08741-2.
5. Olivera, N.A.; Ranke, P.J. Theoretical aspects of the magnetocaloric effect. *Phys. Rep.* **2010**, *489*, 89–159. [[CrossRef](#)]
6. Ucar, H.; Ipus, J.J.; Laughlin, D.E.; McHenry, M.E. Tuning the Curie temperature in  $\gamma$ -FeNi nanoparticles for magnetocaloric applications by controlling the oxidation kinetics. *J. Appl. Phys.* **2013**, *113*, 17A918. [[CrossRef](#)]
7. Oliveira, N.A. Magnetocaloric effect in transition metals-based compounds: A theoretical approach: A theoretical approach. *Eur. Phys. J. B Condens. Matter Complex Syst.* **2004**, *40*, 259–264. [[CrossRef](#)]
8. Franco, V.; Blázquez, J.S.; Opus, J.J.; Law, J.Y.; Moreno, L.M.; Conde, A. Magnetocaloric effect: From materials research to refrigeration devices. *Prog. Mater. Sci.* **2018**, *93*, 112–232. [[CrossRef](#)]

9. Romero, J.; Ferreira, R.; De Miguel, A.; Romero, M. Magnetocaloric effect: A review of the thermodynamic cycles in magnetic refrigeration. *Renew. Sustain. Energy Rev.* **2013**, *17*, 74–82. [[CrossRef](#)]
10. Phan, M.-H.; Yu, S.-C. Review of the magnetocaloric effect in manganite materials. *J. Magn. Magn. Mater.* **2007**, *308*, 325–340. [[CrossRef](#)]
11. Chaudhary, V.; Chen, X.; Ramanujan, R.V. Iron and manganese based magnetocaloric materials for near room temperature thermal management. *Prog. Mater. Sci.* **2019**, *100*, 64–98. [[CrossRef](#)]
12. Xu, P.; Hub, L.; Zhang, Z.; Wang, H.; Li, L. Electronic structure, magnetic properties and magnetocaloric performance in rare earths (RE) based RE<sub>2</sub>BaZnO<sub>5</sub> (RE = Gd, Dy, Ho, and Er) compounds. *Acta Mater.* **2022**, *236*, 118114. [[CrossRef](#)]
13. Zhang, Y.; Li, S.; Hu, L.; Wang, X.; Li, L.; Yan, M. Excellent magnetocaloric performance in the carbide compounds RE<sub>2</sub>Cr<sub>2</sub>C<sub>3</sub> (RE = Er, Ho, and Dy) and their composites. *Mater. Today Phys.* **2022**, *27*, 100786. [[CrossRef](#)]
14. Lyubina, J. Magnetocaloric materials for energy efficient cooling. *J. Phys. D Appl. Phys.* **2017**, *50*, 053002. [[CrossRef](#)]
15. Sharma, M.K.; Mukherjee, K. Evidence of large magnetic cooling power and double glass transition in Tb<sub>5</sub>Pd<sub>2</sub>. *J. Magn. Magn. Mater.* **2018**, *466*, 317–322. [[CrossRef](#)]
16. Sharma, M.K.; Yadav, K.; Mukherjee, K. Complex magnetic behaviour and evidence of superspin glass state in the binary intermetallic compound Er<sub>5</sub>Pd<sub>2</sub>. *J. Phys. Condens. Matter* **2018**, *30*, 215803. [[CrossRef](#)] [[PubMed](#)]
17. Biswas, A.; Chandra, S.; Samanta, T.; Phan, M.H.; Das, I.; Srikanth, H. The universal behavior of inverse magnetocaloric effect in antiferromagnetic materials. *J. Appl. Phys.* **2013**, *113*, 17A902. [[CrossRef](#)]
18. Sharma, M.K.; Mukherjee, K. Magnetic and universal magnetocaloric behavior of rare-earth substituted DyFe<sub>0.5</sub>Cr<sub>0.5</sub>O<sub>3</sub>. *J. Magn. Magn. Mater.* **2017**, *444*, 178–183. [[CrossRef](#)]
19. Sharma, M.K.; Kaur, G.; Mukherjee, K. Nature of glassy magnetic state in magnetocaloric materials Dy<sub>5</sub>Pd<sub>2-x</sub>Ni<sub>x</sub> (x = 0 and 1) and universal scaling analysis of R<sub>5</sub>Pd<sub>2</sub> (R = Tb, Dy and Er). *J. Alloys Compd.* **2019**, *782*, 10–16. [[CrossRef](#)]
20. Xuexi Zhang, X.; Zhang, H.; Qian, M.; Geng, L. Enhanced magnetocaloric effect in Ni-Mn-Sn-Co alloys with two successive magnetocrystallographic transformations. *Sci. Rep.* **2018**, *8*, 8235. [[CrossRef](#)]
21. Sarkar, S.K.; Babu, P.D.; Biswas, A.; Siruguri, V.; Krishnan, M. Giant magnetocaloric effect from reverse martensitic transformation in Ni-Mn-Ga-Cu ferromagnetic shape memory alloys. *J. Alloys Compd.* **2016**, *670*, 281–288. [[CrossRef](#)]
22. Umetsu, R.Y.; Kusakari, Y.; Kanomata, T.; Suga, K.; Sawai, Y.; Kindo, K.; Oikawa, K.; Kainuma, R.; Ishida, K. Metamagnetic behaviour under high magnetic fields in Ni<sub>50</sub>Mn<sub>50-x</sub>In<sub>x</sub> (x = 14.0 and 15.6) shape memory alloys. *J. Phys. D Appl. Phys.* **2009**, *42*, 075003. [[CrossRef](#)]
23. Chaudhary, V.; Ramanujan, R.V. Magnetic and structural properties of high relative cooling power (Fe<sub>70</sub>Ni<sub>30</sub>)<sub>92</sub>Mn<sub>8</sub> magnetocaloric nanoparticles. *J. Phys. D Appl. Phys.* **2015**, *48*, 305003. [[CrossRef](#)]
24. Ucar, H.; Craven, M.; Laughlin, D.E.; McHenry, M.E. Effect of Mo addition on structure and magnetocaloric effect in γ-FeNi nanocrystals. *J. Electron. Mater.* **2014**, *43*, 137–141. [[CrossRef](#)]
25. Chaudhary, V.; Ramanujan, R.V. Magnetocaloric Properties of Fe-Ni-Cr Nanoparticles for Active Cooling. *Sci. Rep.* **2016**, *6*, 35156. [[CrossRef](#)] [[PubMed](#)]
26. Sarlar, K.; Tekgul, A.; Küçük, N.; Etemoğlu, A.B. Structural and magnetocaloric properties of FeNi high entropy alloys. *Phys. Scr.* **2021**, *96*, 125847. [[CrossRef](#)]
27. Kurlyandskaya, G.V.; Bhagat, S.M.; Bagazeev, A.V.; Medvedev, A.I.; Ballesteros, A.; Beketov, I.V.; Safronov, A.P. Structure, magnetic and microwave properties of FeNi invar nanoparticles obtained by electrical explosion of wire in different preparation conditions. *J. Phys. Chem. Solids* **2016**, *98*, 255–262. [[CrossRef](#)]
28. Chaudhary, V.; Ramanujan, R.V. High Relative Cooling Power in a Multiphase Magnetocaloric FeNiB Alloy. *IEEE Magn. Lett.* **2015**, *6*, 6700104. [[CrossRef](#)]
29. Paduani, C.; Krause, J.C. Local magnetic properties of γ-Fe-Mn alloys. *Phys. Rev. B* **1998**, *58*, 175–179. [[CrossRef](#)]
30. Kumari, K.; Kumar, A.; Shin, M.; Kumar, S.; Huh, S.H.; Koo, B.H. Investigating the magnetocrystalline anisotropy and the exchange bias through interface effects of nanocrystalline FeCo. *J. Korean Phys. Soc.* **2021**, *79*, 1180–1189. [[CrossRef](#)]
31. Kumari, K.; Kumar, A.; Koo, B.H. Investigating the origin of exchange bias effect in ferromagnetic FeNi nanoparticles prepared via controlled synthesis. *Appl. Nanosci.* **2021**, 1–9. [[CrossRef](#)]
32. Ghisari, K.; Oh, J.T.; Javapour, S. The effect of heat treatment on the structure and magnetic properties of mechanically alloyed Fe–45%Ni nanostructured powders. *J. Alloys Compd.* **2011**, *509*, 1020–1024. [[CrossRef](#)]
33. Sharma, M.K.; Kumar, A.; Kumari, K.; Park, S.-J.; Yadav, N.; Huh, S.-H.; Koo, B.-H. Structural, Magnetic, and Magnetocaloric Studies of Ball-Milled Fe<sub>100-x</sub>T<sub>x</sub> (T = Ni and Mn) Alloy. *Appl. Sci.* **2022**, *12*, 9098. [[CrossRef](#)]
34. Vas'kovskiy, V.O.; Lepalovskij, V.N.; Gor'kovenko, A.N.; Kulesh, N.A.; Savin, P.A.; Svalov, A.V.; Stepanova, E.A.; Shchegoleva, N.N.; Yuvchenko, A.A. Fe<sub>20</sub>Ni<sub>80</sub>/Fe<sub>50</sub>Mn<sub>50</sub> Film Magnetoresistive Medium. *Tech. Phys.* **2015**, *60*, 116–122. [[CrossRef](#)]
35. Gor'kovenko, A.N.; Lepalovskij, V.N.; Savin, P.A.; Vas'kovskiy, V.O. Effect of Technological Conditions on the Magnetic and Magnetoresistive Properties of Fe<sub>20</sub>Ni<sub>80</sub>/Fe<sub>50</sub>Mn<sub>50</sub> Films. *Bull. Russ. Acad. Sci. Phys.* **2014**, *78*, 925–926. [[CrossRef](#)]
36. Swartzendruber, L.J.; Itkin, V.P.; Alcock, C.B. The Fe-Ni (Iron-Nickel) system. *J. Phase Equilibria Diffus.* **1991**, *12*, 288–312. [[CrossRef](#)]
37. Miettinen, J.; Lilova, K.; Vassilev, G. Thermodynamic Description of Ternary Fe-B-X Systems. Part 3: Fe-B-Mn. *Arch. Metall. Mater.* **2014**, *59*, 1481–1485. [[CrossRef](#)]

38. Miettinen, J.; Lilova, K.; Vassilev, G. Thermodynamic description of ternary Fe-B-X systems. Part 2: Fe-B-Ni. *Arch. Metall. Mater.* **2014**, *59*, 609–614. [[CrossRef](#)]
39. Witusiewicz, V.T.; Sommer, F.; Mittemeijer, E.J. Reevaluation of the Fe-Mn Phase Diagram. *J. Phase Equilibria Diffus.* **2004**, *25*, 346–354. [[CrossRef](#)]
40. Sun, X.; Zhu, X.; Ruan, Y.R.; Ding, Z.L.; Song, W.H.; Zhao, B.C.; Ma, Y.Q. NiFe<sub>2</sub> and its nitride g-NiFe<sub>2</sub>N derived from NiFe<sub>2</sub>O<sub>4</sub>: Magnetostriction, thermal expansion, resistivity and corrosion resistance. *Mater. Res. Bull.* **2017**, *89*, 245–252. [[CrossRef](#)]
41. Valenzuela, J.L.; Valderruten, J.F.; Alcázar, G.P.; Colorado, H.D.; Romero, J.J.; González, J.M.; Greneche, J.M.; Marco, J.F. Low temperature study of mechanically alloyed Fe<sub>67.5</sub>Ni<sub>32.5</sub> Invar sample. *J. Magn. Magn. Mater.* **2015**, *385*, 83–87. [[CrossRef](#)]
42. Abdu, Y.A.; Ericsson, T.; Annersten, H. Coexisting antiferromagnetism and ferromagnetism in mechanically alloyed Fe-rich Fe–Ni alloys: Implications regarding the Fe–Ni phase diagram below 400 °C. *J. Magn. Magn. Mater.* **2004**, *280*, 395–403. [[CrossRef](#)]
43. Rancourt, D.G.; Hargraves, P.; Lamarch, G. Microstructure and Low Temperature Magnetism of Fe-Ni Invar Alloys. *J. Magn. Magn. Mater.* **1990**, *87*, 71–82. [[CrossRef](#)]
44. Rancourt, D.G.; Scorzelli, R.B. Low spin  $\gamma$ -Fe-Ni( $\gamma_{LS}$ ) proposed as a new mineral in Fe-Ni bearing meteorites: Epitaxial intergrowth of  $\gamma_{LS}$  and tetrataenite as a possible equilibrium state at 20–40 at% Ni. *J. Magn. Magn. Matter.* **1995**, *150*, 30–36. [[CrossRef](#)]
45. Kumar, A.; Kumari, K.; Sharma, M.K.; Vij, A.; Kumar, S.; Huh, S.H.; Koo, B.H. Chemically inducing room temperature spin-crossover in double layered magnetic refrigerants Pr<sub>1.4+x</sub>Sr<sub>1.6-x</sub>Mn<sub>2</sub>O<sub>7</sub> (0.0 ≤ x ≤ 0.5). *J. Mater. Sci. Technol.* **2022**, *124*, 232–242. [[CrossRef](#)]
46. Rodriguez-Carvajal, J. FULLPROF: A Program for Rietveld Refinement and Pattern Matching Analysis. In *Abstracts of the Satellite Meeting on Powder Diffraction of the XV Congress of the IUCr*; IUCr: Toulouse, France, 1990; p. 127.
47. Rodriguez-Carvajal, J. Recent Advances in Magnetic Structure Determination by Neutron Powder Diffraction. *Phys. B* **1993**, *192*, 55–69; Recent Developments of the Program FULLPROF, in Commission on Powder Diffraction (IUCr). *Newsletter* **2001**, *26*, 12–19. [[CrossRef](#)]
48. Rodríguez, V.P.; Rojas-Ayala, C.; Medina, J.M.; Cabrera, P.P.; Quispe-Marcotoma, J.; Landauro, C.V.; Rojas Tapia, J.; Baggio-Saitovitch, E.M.; Passamani, E.C. Fe<sub>50</sub>Ni<sub>50</sub> synthesized by high energy ball milling: A systematic study using X-ray diffraction, EXAFS and Mössbauer methods. *Mater. Charact.* **2019**, *149*, 249–254. [[CrossRef](#)]
49. Reuter, K.B.; Williams, D.B.; Goldstein, J.I. Determination of the Fe–Ni phase diagram below 400 °C. *Metall. Mater. Trans. A* **1989**, *20*, 719–725. [[CrossRef](#)]
50. Byshkin, M.; Hou, M. Phase transformations and segregation in Fe–Ni alloys and nanoalloys. *J. Mater. Sci.* **2012**, *47*, 5784–5793. [[CrossRef](#)]
51. Dung Nguyen-Trong, D.; Pham-Huu, K.; Nguyen-Tri, P. Simulation on the Factors Affecting the Crystallization Process of FeNi Alloy by Molecular Dynamics. *ACS Omega* **2019**, *4*, 14605–14612. [[CrossRef](#)]
52. Nguyen, T.D. Influence of impurity concentration, atomic number, temperature and tempering time on microstructure and phase transformation of Ni<sub>1-x</sub>Fe<sub>x</sub> (x = 0.1, 0.3, 0.5) nanoparticles. *Mod. Phys. Lett. B* **2018**, *32*, 1850204.
53. Huck, B.; Hesse, J. Search for Reentrant Spin Glass Phenomenon in the “Classic” FeNi-Invar. *J. Magn. Magn. Mater.* **1987**, *70*, 425–426. [[CrossRef](#)]
54. Rancourt, D.G.; Hargraves, P.; Lamarch, G. Reentrant Magnetism, Antiferromagnetism, and Domain Wall Pinning in Nominally Ferromagnetic Fe-Ni Invar. *J. Magn. Magn. Mater.* **1989**, *78*, 129–152. [[CrossRef](#)]
55. Banerjee, B.K. On a generalised approach to first and second order magnetic transitions. *Phys. Lett.* **1964**, *12*, 16–17. [[CrossRef](#)]
56. Liu, X.B.; Altounian, Z. Magnetocaloric effect in (Er<sub>1-x</sub>Gd<sub>x</sub>)Co<sub>2</sub> pseudobinary compounds. *J. Magn. Magn. Mater.* **2005**, *292*, 83–88. [[CrossRef](#)]
57. Olivier Toulemonde, O.; Roussel, P.; Isnard, O.; Andre, G.; Mentre, O. Spin-Flop Transition and Magnetocaloric Effect through Disconnected Magnetic Blocks in CoIII/CoIV Oxybromides. *Chem. Mater.* **2010**, *22*, 3807–3816. [[CrossRef](#)]
58. M’assri, R. Magnetocaloric effect and its implementation in critical behaviour study of La<sub>0.67</sub>Ca<sub>0.33</sub>Mn<sub>0.9</sub>Fe<sub>0.1</sub>O<sub>3</sub>. *Bull. Mater. Sci.* **2016**, *39*, 551–557. [[CrossRef](#)]
59. Franco, V.; Blazquez, J.S.; Conde, A. Field dependence of the magnetocaloric effect in materials with a second order phase transition: A master curve for the magnetic entropy change. *Appl. Phys. Lett.* **2006**, *89*, 222512. [[CrossRef](#)]

**Disclaimer/Publisher’s Note:** The statements, opinions and data contained in all publications are solely those of the individual author(s) and contributor(s) and not of MDPI and/or the editor(s). MDPI and/or the editor(s) disclaim responsibility for any injury to people or property resulting from any ideas, methods, instructions or products referred to in the content.